RSC Advances

PAPER

View Article Online
View Journal | View Issue

Cite this: *RSC Adv.*, 2014, **4**, 55162

Synthesis, characterization and application of amino-functionalized multi-walled carbon nanotubes for effective fast removal of methyl orange from aqueous solution†

Yan Liu, Guijia Cui, Chao Luo, Li Zhang, Yaopeng Guo and Shiqiang Yan*

Received 9th September 2014
Accepted 20th October 2014

DOI: 10.1039/c4ra10047f

www.rsc.org/advances

Amino-functionalized multi-walled carbon nanotubes (NH_2-MWCNTs) for the removal of methyl orange (MO) from aqueous solution were prepared for the first time using 1,6-hexanediamine by a simple one-pot process at 198 °C for 8 h. The resulting materials were characterized by different techniques, such as TEM, FTIR, XPS, Raman, elemental analysis and BET surface area measurement. Experimental results indicated that the amount of 1,6-hexanediamine bound on MWCNTs was estimated to be around 5 wt% and the materials showed an excellent adsorption capacity (q_{max} = 185.53 mg g^{-1}). The adsorption equilibrium could be reached within 10 min. Both Langmuir and Freundlich models showed a better fit with experimental data than the Temkin model and the adsorption kinetics could be accurately described by the pseudo-second-order model. The overall rate process was jointly controlled by intra-particle diffusion and external mass transfer. Moreover, the thermodynamic parameters indicated that the adsorption was spontaneous and exothermic. Results of this work are of great importance for environmental applications of amino-functionalized multi-walled carbon nanotubes as promising dye adsorbents in wastewater treatment.

1. Introduction

Water is the most important and essential component on the earth for vital activities of living beings. Unfortunately, in recent years, a considerable amount of wastewater has been produced from a wide range of industries, including textile, printing, paper, dyestuff, plastic and other industries.[1–3] The release of effluents with high color and high suspended organic solids into the environment imposes serious environmental threats because it is rather difficult to treat dye wastewater due to the non-biodegradable and polluting nature of the pollutants.[4–7] Apart from these dyes are also toxic for environments and humans, they are also known to affect the central nervous system, which makes their removal from wastewater a major environmental issue.[8–12]

For the benefit of human health and ecological security, new methods to remove dyes from the colored effluents are urgently needed, and also should be cheap, effective and environmentally friendly. Among various physical, chemical and biological conventional removal process, adsorption technology is one of the most effective methods due to its low costs, high efficiency and easy operation.[13–16] Up to now, various natural and synthetic adsorbents have been studied, such as banana peel,[17] orange peel,[17] activated carbon,[18] chitosan/MgO composite[19] and various nanotubes.[20,21] However, the application of the sorbents has some inherent limitations, such as the long elapsed time and low adsorption capacity. Thus, developing new adsorbents with simple synthesis, high adsorption capacity and low-cost, is highly desired.

Among many kinds of carbon materials, which have been prepared and used for the removal of dyes and heavy metal ions, carbon nanotubes (CNTs), which were originally discovered by Iijima and included single-walled and multi-walled CNTs (MWCNTs), are relatively new materials that have been attracting great attention due to their excellent mechanical, electrical, optical, physical, and chemical properties.[22–29] However, the application of CNTs has been significantly hindered by their poor dispersion into solvents because of the strong intermolecular van der Waals interactions among tubes, which can lead to the formation of aggregates.[30] To improve the dispersion and realize the great capability of CNTs, researchers have applied various kinds of treatment approaches to generate new functional groups on the surface of CNTs. Among these methods, amino-functionalized CNTs have been investigated because amino group has a high reactivity, and can react with many chemicals.[31,32] Nevertheless, to the best of our knowledge, few investigations have focused on the adsorption of dyes on

College of Chemistry and Chemical Engineering, Lanzhou University, Lanzhou 730000, PR China. E-mail: yansq@lzu.edu.cn; Fax: +86-931-8912582; Tel: +86-931-8912582

† Electronic supplementary information (ESI) available. See DOI: 10.1039/c4ra10047f

amino-functionalized CNTs and simultaneously determined the kinetics equilibrium and thermodynamic parameters thus far.

In this paper, amino-functionalized multi-walled carbon nanotubes (NH_2-MWCNTs) were first prepared by a facile one-pot method using 1,6-hexanediamine (HDA), and the nanocomposite was characterized using transmission electron microscopy (TEM), Fourier-transform infrared spectroscopy (FTIR) analysis, Raman, X-ray photoelectron spectroscopy (XPS), elemental analyser, X-ray diffraction (XRD), Brunauer, Emmett, and Teller surface area measurement (BET) analyses. This work is a successful attempt to explore new method to prepare amino-functionalized MWCNTs and the new simple method may be further used to develop other promising carbon materials for possible application. And its adsorption capability for organic pollutants was investigated using methyl orange (MO) as a model. Moreover, the adsorption kinetics, rate-controlling mechanisms, and thermodynamic parameters of the adsorbents were also investigated to evaluate these adsorption behaviors further. This information may be very useful for further research and practical applications of the adsorbent in dyeing wastewater treatment.

2. Experimental

2.1 Materials

MWCNTs with an external diameter of 20–30 nm, length of 5–20 μm, specific surface area of over 200 $m^2\ g^{-1}$, were purchased from Alpha Nano Technology Co., Ltd. (China). The purity of the MWCNTs, referred to as "raw-MWCNTs," was more than 95%.

2.2 Preparation of material

The raw-MWCNTs were dispersed in 100 mL concentrated HNO_3 and sonicated for 1 h, and then oxidized at 120 °C for 2 h (Scheme 1). The resulting MWCNTs were washed with deionized water and ethanol absolute for several times, and then dried at 80 °C for 12 h. These materials were denoted as "o-MWCNTs."

2.3 Preparation of NH_2-MWCNTs

1,6-Hexanediamine was grafted onto o-MWCNTs surfaces *via* a simple solvothermal reaction. Briefly, 100 mg of o-MWCNTs were dispersed in ethylene glycol (EG) under ultrasonication, followed by the addition of 1,6-hexanediamine (HDA, 6.5 g). Afterwards, the dark brown mixture was stirred vigorously for 30 min before transferred into a Teflon-lined stainless steel autoclave; thereafter, the autoclave was healed at 198 °C for 8 h and allowed to cool to room temperature (Scheme 1). The resultant product was filtered, washed repeatedly with distilled water and ethanol, and then dried at 60 °C for further usage.

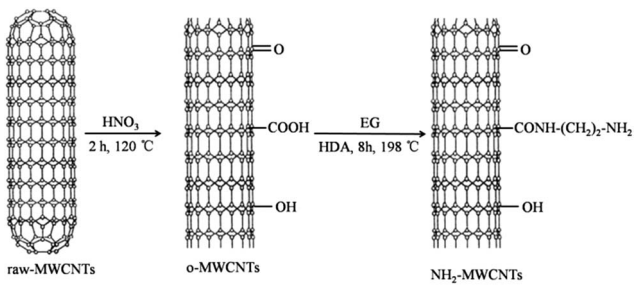

Scheme 1 Schematic presentation of the functionalization of MWCNTs.

2.4 Characterization of MWCNTs

The morphology of o-MWCNTs and NH_2-MWCNTs was examined on a transmission electron microscope (TEM, TecnaiG2F30). The functional groups of the raw-MWCNTs, o-MWCNTs, and NH_2-MWCNTs were examined using a NEXUS 670 FTIR spectrometer (Nicolet Instrument Corporation, USA) with KBr pellets containing the samples. The Raman spectra were recorded on a Dilor LABRAM-1B multichannel confocal microspectrometer with 514 nm laser excitation. X-ray photoelectron spectroscopy (XPS) spectra were obtained with an ESCALab220i-XL electron spectrometer (VG Scientific) using 300 W Al Kα radiation. A VarioEL element analyzer, elementar Analysensysteme GmbH (Hanau, Germany), was used for elemental analysis. The inorganic phases of the o-MWCNTs and NH_2-MWCNTs were examined using X-ray diffraction (XRD; XRD-6000, Shimadzu, Japan). The BET surface area, pore volume, and pore size were characterized using nitrogen adsorption at liquid nitrogen temperatures (Sorptomatic 1990, Thermo, USA).

2.5 Adsorption experiments

Analytical grade methyl orange was used to prepare a 1000 mg L^{-1} stock solution, which was further diluted to the required concentration before use.

To observe the effect of NH_2-MWCNTs dose on dyes adsorption, different amounts of adsorbent (varying from 0.16 g L^{-1} to 0.4 g L^{-1}) were respectively added into fixed initial concentration of MO solution at 298 K at pH 7 until the equilibrium time was reached. The two phases were separated by filtration using a 0.45 μm microporous membrane filter. The finial MO concentrations remaining in the solution were analyzed by spectrophotometric method at 465 nm.

To determine the adsorption capacities of NH_2-MWCNTs compared with other materials, the raw-MWCNTs, o-MWCNTs, and NH_2-MWCNTs were prepared as adsorbents for MO removal. The samples of different adsorbents were added to each 25 mL of MO solutions with initial concentration of 10 mg L^{-1} to 60 mg L^{-1} (10 mg L^{-1} intervals). In the subsequent experiments, NH_2-MWCNTs were chosen as the adsorbent in the following experiments and were kept constant.

The effect of pH on MO adsorption was studied by varying the solution pH from 2.0 to 10.0, with the initial MO concentration of 60 mg L^{-1}. The pH of the samples was adjusted by adding 1 M HCl or NaOH to each solution.

In the experiments on the effect of temperature, the temperature was held at three different temperatures (273, 298, and 313 K) with different concentrations. The amount of MO

adsorption at equilibrium q_e (mg g^{-1}) was calculated using the following equation:

$$q_e = \frac{V(C_0 - C_e)}{W} \quad (1)$$

where C_0 and C_e (mg L^{-1}) are the liquid phase concentrations of dye at initial and equilibrium, respectively, V (L) the volume of the solution and W (g) is the mass of adsorbent used.

Adsorption kinetic samples were prepared by adding 1 g of NH_2-MWCNTs into a 2000 mL solution. Samples were collected at predetermined time intervals using a membrane filter.

3. Results and discussion

3.1 Characterization of different materials

The morphology of o-MWCNTs and NH_2-MWCNTs are examined by TEM under different magnifications and representative images are shown in Fig. 1. The sample does not differ significantly from its original shape, which suggests that amine modification did not alter the nanotube structure. Compared with o-MWCNTs, sidewalls of amino-functionalized MWCNTs seemed to be more corrugated.

The FTIR spectra of raw-MWCNTs, o-MWCNTs and NH_2-MWCNTs are compared in Fig. 2. The HNO_3 treatment produced carboxyl groups on the external surface of the MWCNTs because of oxidation, as showed by the characteristic peaks at 3429 and 1725 cm^{-1} of the stretching vibrations of ν(OH) and ν(C=O) of the carboxylic groups (COOH), respectively. The bands within the 1650 cm^{-1} to 1550 cm^{-1} range are associated with the C=O groups under different environments (ketone/quinone), as well as with the C=C in aromatic rings; whereas the bands within the 1200 cm^{-1} to 1000 cm^{-1} range have proven the presence of C–O bonds in various chemical surroundings.[23] The FTIR transmission spectrum of NH_2-MWCNTs changed obviously after amine modification. The presence of new peaks at 1158 and 1255 cm^{-1} matched well with N–H in-plane and C–N stretching vibration, respectively. In addition, a band at ≈800 cm^{-1} corresponded to the out-of-plane NH_2 bending mode.[31,33] The FTIR results indicated that amino groups were successfully attached onto the surface of the MWCNTs. All of these functional groups can act as the sorption sites and thereby increase the sorption capacity of amino-functionalized MWCNTs.

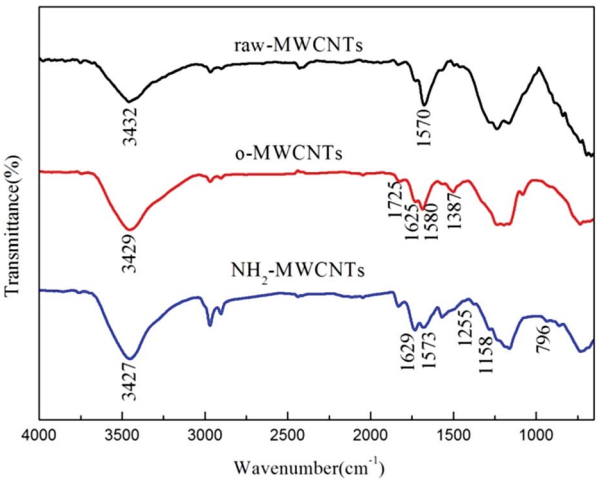

Fig. 2 FTIR transmission spectra of raw-MWCNTs, o-MWCNTs and NH_2-MWCNTs.

The Raman spectra of MWCNTs presented in Fig. 3 are composed of two strong characteristic peaks. The peak near 1350 cm^{-1} is an indication of disordered sp^2-hybridized carbon atoms of nanotubes containing vacancies, or other symmetry-breaking defects and labelled as the D-band. The peak observed around 1580 cm^{-1}, which is called the G band, is ascribed to the E_{2g} symmetry of the interlayer mode reflecting structural integrity of sp^2-hybridized carbon atoms of the nanotubes. The intensity ratio of D to G band (I_D/I_G) is generally accepted to reflect the extent of carbon-containing defects of carbon materials.[34] The I_D/I_G of raw-MWCNTs is about 0.89. After treatment with HNO_3, the I_D/I_G of o-MWCNTs is increased to 1.10, meaning that more carbon-containing defects appeared

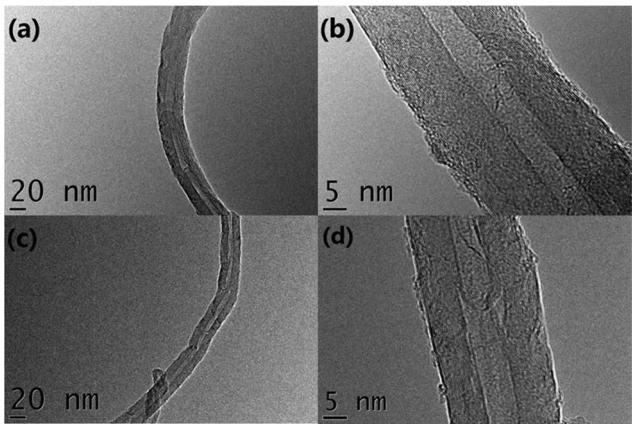

Fig. 1 Representative TEM images of o-MWCNTs and NH_2-MWCNTs under different magnifications. Images (a) to (b) refer to o-MWCNTs and (c) to (d) refer to NH_2-MWCNTs.

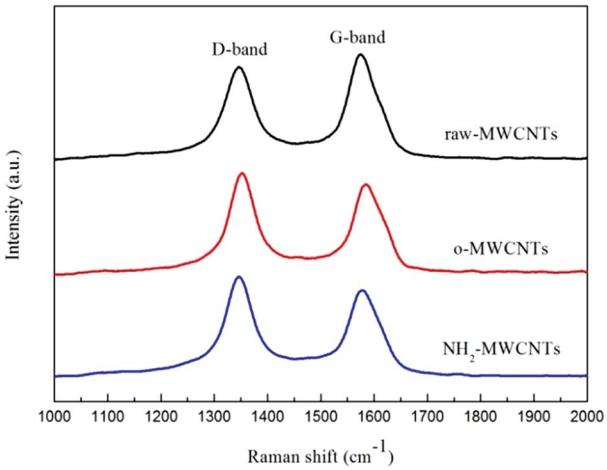

Fig. 3 Raman spectra of raw-MWCNTs, o-MWCNTs and NH_2-MWCNTs.

on the surface of o-MWCNTs, which introduced more surface oxygen groups as shown in FTIR spectra. Compared to o-MWCNTs, the D band of NH_2-MWCNTs is slightly shifted downward, and the I_D/I_G is slightly increased to 1.20. These phenomena could be attributed to the decrease of the ordered graphite crystal structure of NH_2-MWCNTs after conjugating with HDA. The existence of amino and hydroxyl groups in the MWCNTs would be further confirmed by XPS and elemental analysis.

The composition of NH_2-MWCNTs was determined by XPS as shown in Fig. 4, and peaks of C, O, and N can be found in Fig. 4a. The C 1s peak is decomposed into three distinct peaks at 283.7, 284.45 and 286.1 eV (Fig. 4a), corresponding to graphitic carbon, C–OH, C–N,[35,36] respectively. The O 1s peak was fitted with five different components (Fig. 4b). Compared with the reported values in literatures,[37,38] the peak at 530.6 eV could be ascribed to adventitious oxygen; the peaks located at 531.5 and 533.5 eV were due to O–C=O; the peak at 532.4 eV corresponded to O=C–N; the peak centered at 532.95 eV derived from the contribution of C–C=O. More importantly, the amine is identified in the N 1s spectrum in Fig. 3d, and the exclusively single peak with binding energy of 399.2 eV can be assigned to primary amine C–NH_2 bonding with carbon.[39]

The attachment of amine at the surface of NH_2-MWCNTs was further confirmed by elemental analysis, which indicated C, 82.02; N, 1.20; H, 1.19% in the materials. Based on the results, the amount of 1,6-hexanediamine bound on MWCNTs is estimated to be around 5 wt% from the percentage of nitrogen. In a word, the aforementioned results verify that the amino groups are successfully conjugated with MWCNTs.

The typical XRD patterns of o-MWCNTs and NH_2-MWCNTs are presented in Fig. S1.† A sharp peak and a broad weak peak can be seen at $2\theta = 25.94°$ and $2\theta = 43.46°$, respectively, which assigned to the distance between walls in MWCNTs and the interwall spacing as well.[40] After surface modification, the NH_2-MWCNTs still had the same cylinder wall structure as o-MWCNTs. The results suggested that the modification process did not change the structural sidewalls of MWCNTs.

The physical properties of o-MWCNTs and NH_2-MWCNTs are summarized in Table 1. The surface area of o-MWCNTs was much smaller than that of raw-MWCNTs ($\geq$200 m^2 g^{-1}). The reasons that make this difference are that the length of o-MWCNTs became shorter and the confined space among isolated MWCNTs appeared narrower than raw-MWCNTs. An evident increase in the structural parameters is shown after amino-functionalized. This could be explained if the high temperature treatment used during the modification resulted in smaller aggregates of NH_2-MWCNTs.

3.2 Adsorption experiment studies

3.2.1 Effect of NH_2-MWCNTs dose on MO adsorption. The adsorbent dose determines the capacity of sorbent for a given initial concentration of adsorbate solution, so it is an important parameter in adsorption processes. The effect of NH_2-MWCNTs dose on the adsorption of MO is presented in Fig. 5. Analysis of Fig. 5 demonstrated that the adsorption removal percentage of MO increased with increasing adsorbent amount. Increasing the dose of NH_2-MWCNTs would increase the number of available adsorption sites, thereby resulting in the increase in removal percentage of MO. However, the adsorption capacity increased at first but then dropped as the dosage increased, and the former trend was caused by the availability of more surface area for dye at low doses in the solution while increasing the dosage increases the possibility of the NH_2-MWCNTs entanglement at high doses. Furthermore, the high dosage may affect the physical properties of the solid–liquid suspensions

Table 1 Surface characteristics of different materials

Materials	Surface area (m^2 g^{-1})	Pore volume (cm^3 g^{-1})	Pore size (nm)
o-MWCNTs	120.07	0.438	14.29
NH_2-MWCNTs	159.69	0.769	19.27

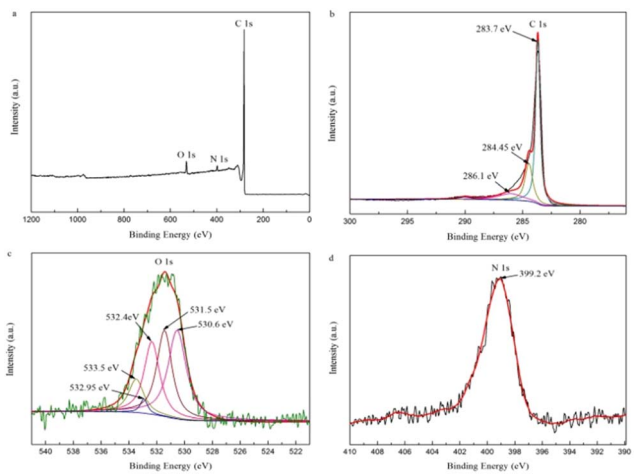

Fig. 4 The XPS analysis of NH_2-MWCNTs: (a) survey spectrum; (b) C 1s spectrum; (c) O 1s spectrum; (d) N 1s spectrum.

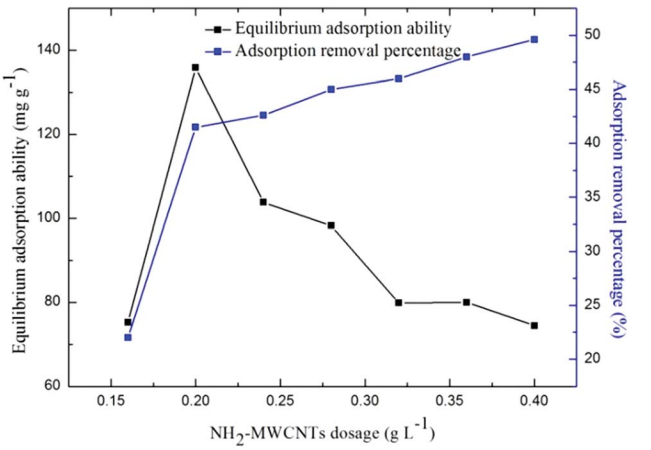

Fig. 5 Effect of adsorbent dose on the adsorption of MO by NH_2-MWCNTs (experimental conditions: initial dye concentration: 60 mg L^{-1}, temperature: 293 K, contact time: 2 h).

including their viscosity. Roughly similar results were also obtained for neem leaf powder by Bhattacharyya and Sharma and for cross-linked chitosan beads by Chiou *et al.*[41,42]

3.2.2 Adsorption capacities of different materials. Fig. 6 shows the adsorption capacities of NH_2-MWCNTs compared with other materials. The adsorption capacity of o-MWCNTs is lower than that of raw-MWCNTs, which can be due largely to the electrostatic repulsions between anionic dyes and partially negative charged o-MWCNTs because of the presence of oxygen-containing functional groups. In addition, the relatively lower specific surface area of o-MWCNTs also influences the adsorption process. It can be noticed that NH_2-MWCNTs show best sorption capacity among the three kinds of materials, indicating that amino functional groups provide more binding sites for MO compared with other materials. Therefore, the adsorption capacities of different materials mainly depend on the functional groups, as well as on the physical properties of the adsorbents.

3.2.3 Effect of solution pH. MO has two different chemical structures, whose chromophores are anthraquinone or azo bond depending on the pH of the solution.[43] The solution pH has a marked impact on adsorptive uptake of adsorbate molecule presumably on account of its effect on the surface properties of the adsorbent and the degree of ionization/dissociation of the adsorbate molecule. Fig. 7 clearly indicates that with increase in pH from 2.0 to 10.0, adsorption capacity decreases from 216.26 mg g^{-1} to 77.78 mg g^{-1}. At lower pH, abundance of hydronium ions (H^+ and H_3O^+) in the solution made the NH_2-MWCNTs surface to be more positively charged, which was attracted to the anionic MO species, enhaucing the ability of adsorption for MO by NH_2-MWCNTs. On the contrary, increase of pH value, which led to increase of the number of negatively charged sites, caused more coulombic repulsion between the negatively charged surface and the dye molecules.[44] Moreover, the lower adsorption of MO with the increase in pH may also be the result of the competition interaction between anionic dye and excess OH^- ions in the solution. Consequently, the adsorption capacities of MO by NH_2-MWCNTs at lower pH are larger than that of at higher pH.

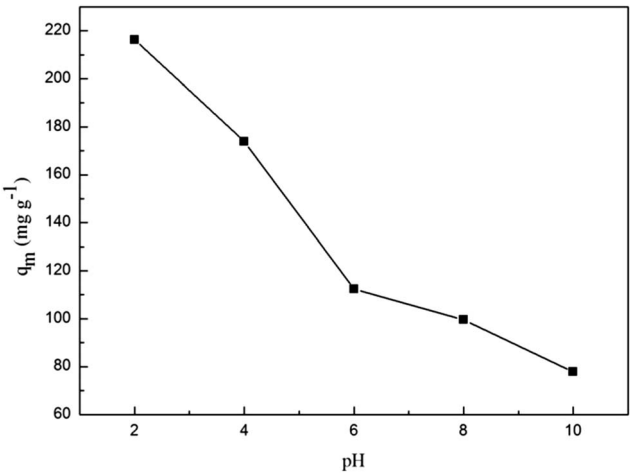

Fig. 7 Effect of solution pH on MO adsorbed onto NH_2-MWCNTs (experimental conditions: initial dye concentration: 60 mg L^{-1}, adsorbents dosage: 5 mg/25 mL, temperature: 293 K, contact time: 2 h).

3.2.4 Effect of contact time and initial concentration. Equilibrium time is one of the most important factors affecting the design of wastewater treatment systems. The effect of adsorption time on the adsorption capacity at the variation of concentrations (20, 40, 60 mg L^{-1}) was studied, as shown in Fig. 8. A close look at Fig. 8 reveals that q_t values increased evidently from 56.35 mg g^{-1} to 127.33 mg g^{-1} as the initial concentration increased from 20 mg L^{-1} to 60 mg L^{-1}, which indicating the important influence of initial solution concentration on the adsorption capacity. The adsorption occurs rapidly at the early stages (contact time <10 min), which may be related to the availability of a large number of vacant active sites on the adsorbent surface. However, with a gradual decrease in

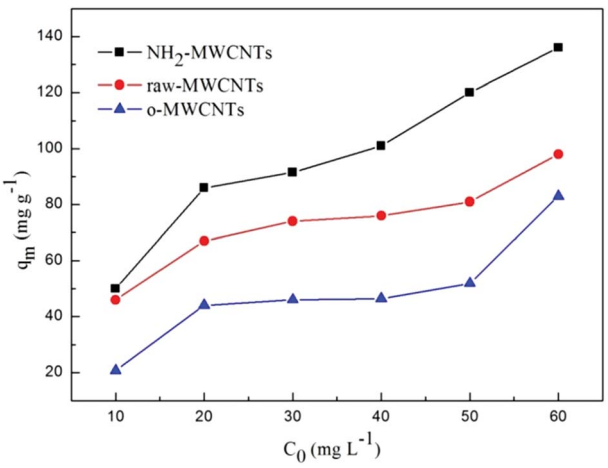

Fig. 6 Adsorption capacities of different materials with regard to MO adsorption (experimental conditions: adsorbents dosage: 5 mg/25 mL, temperature: 293 K, contact time: 2 h).

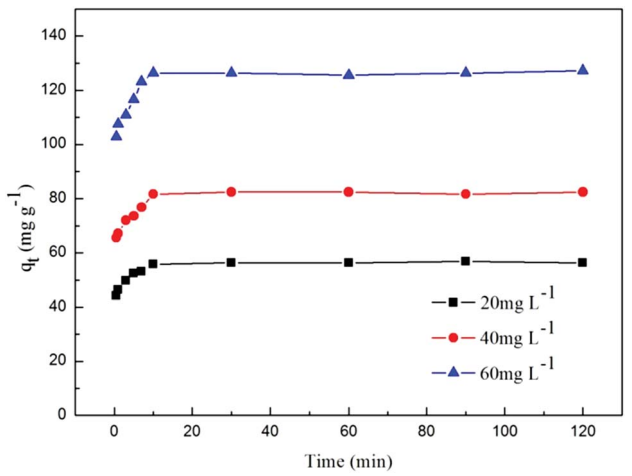

Fig. 8 Effect of contact time on the adsorption of MO by NH_2-MWCNTs (experimental conditions: temperature: 293 K, adsorbent dose: 5 mg/25 mL).

the number of vacant surface sites and an increase of the repulsive forces between the MO molecules on the adsorbent and the bulk phase, eventually, a plateau is reached in all curves.

A further experiments studied the effect of a high range of concentrations (200, 300, 400 mg L^{-1}) on the adsorption capacity were performed as shown in Fig. S2.† The removal of MO increases with increasing contact time and the equilibrium capacity is 196, 305, and 369 mg g^{-1}, respectively, which is much larger than that of low initial concentrations. So when using a higher concentration, the adsorption capacity will become larger. The equilibrium time exhibited small difference as the initial solution concentration increased from 200 mg L^{-1} to 400 mg L^{-1}. The adsorption equilibrium of 200 and 300 mg L^{-1} observed at 30 min and 400 mg L^{-1} initial MO solution almost reached the equilibrium. Although the equilibrium of the adsorption process was observed in a relatively short time, the contact was set at 2 hours in the following each experiments to ensure that the equilibrium was achieved.

3.2.5 Effect of temperature on adsorption capacity. Temperature is of very significance in determining the extent of MO adsorption and batch adsorption studies were performed at three different temperatures on the variation of concentrations at pH 2.0, as shown in Fig. 9. It can be noticed that there was an obvious decrease from 164.21 to 107.56 mg g^{-1} in the adsorption capacity of MO with increase in temperature, which suggests the exothermic nature of the adsorption reaction of MO onto NH_2-MWCNTs. The reasons for this phenomenon may be that the physical bonding between MO molecules and the active sites on the adsorbent surface weakened as temperature increased.

3.2.6 Adsorption isotherms. To optimize the design of an adsorption system, it is important to study the equilibrium data, which are commonly known as adsorption isotherms. Langmuir, Freundlich and Temkin isotherms were applied to describe the adsorption process in this study.

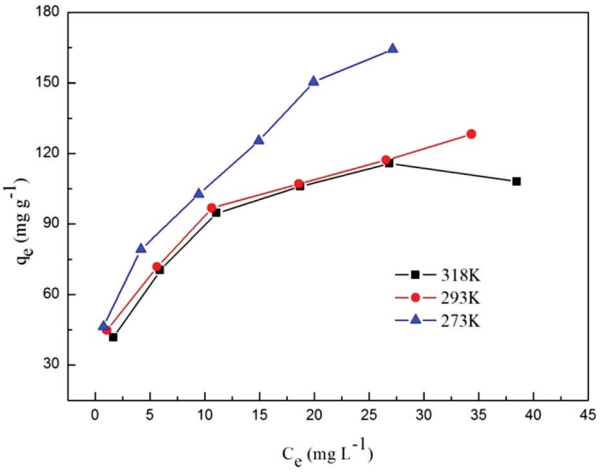

Fig. 9 Effect of temperature on adsorption of MO by NH_2-MWCNTs (experimental conditions: adsorbent dose: 5 mg/25 mL, contact time: 2 h, pH: 2).

The Langmuir model is valid for monolayer adsorption onto a perfectly smooth and homogeneous surface with a finite number of identical sites. It is described by the following equation:[45]

$$\frac{C_e}{q_e} = \frac{1}{bq_m} + \frac{C_e}{q_m} \quad (2)$$

where q_e (mg g^{-1}) is the amount of dye adsorbed per unit mass of the adsorbent at the equilibrium point, C_e (mg L^{-1}) is the equilibrium concentration of MO, q_m (mg g^{-1}) is the maximum adsorbate amount, and b (L mg^{-1}) is the Langmuir constant related to adsorption affinity of the binding sites. When C_e/q_e is plotted *versus* C_e, the q_m and b constants can be calculated from the slope and the intercept (Fig. 10a) and are listed in Table 2. Furthermore, the effect of the isotherm shape was discussed with the aim of understanding whether an adsorption system is favorable or not. Another parameter, R_L, called separation factor or equilibrium parameter, which can be used to express the efficiency of the adsorption, is also evaluated by the following relation:[46]

$$R_L = \frac{1}{1 + bC_0} \quad (3)$$

where b (L mg^{-1}) is the Langmuir constant, and C_0 is the initial MO concentration (mg L^{-1}). The values of R_L indicate the isotherm shapes which can be unfavorable ($R_L > 1$), linear ($R_L = 1$), favorable ($0 < R_L < 1$) or irreversible ($R_L = 0$). As shown in Table 2, the R_L values were found to be in the 0–1 range, which implies the favorable adsorption between NH_2-MWCNTs and MO.

The Freundlich model can be employed to describe heterogeneous surfaces and multilayer adsorption systems, which is generally given as follows:[47]

$$\ln q_e = \ln K_F + \frac{1}{n} \ln C_e \quad (4)$$

where q_e and C_e have the same definitions as those in the Langmuir equation cited above, and K_F and n are the Freundlich constants, which represent the adsorption capacity and the adsorption intensity, respectively. They can be calculated from the intercept and slope of the linear plot of ln q_e *versus* ln C_e (Fig. 10b) and are presented in Table 2. It is generally considered that if the values of n in the range 1–10, the adsorption is favorable. In this research, the sorption is favorable as can be seen in Table 2.

The Temkin model assumes that the heat of adsorption decreases linearly with coverage of the adsorbate and adsorbent interactions and the linear form is expressed as:[48]

$$q_e = B \ln K_T + B \ln C_e \quad (5)$$

where K_T (L mg^{-1}) is the equilibrium binding constant related to the maximum binding energy and B is corresponded to adsorption heat. The values of the parameters are analyzed according to a plot of q_e *versus* ln C_e and are listed in Table 2.

Based on the determination parameters shown in Table 2, both Langmuir and Freundlich models closely fitted the experimental data with good correlation coefficients. The

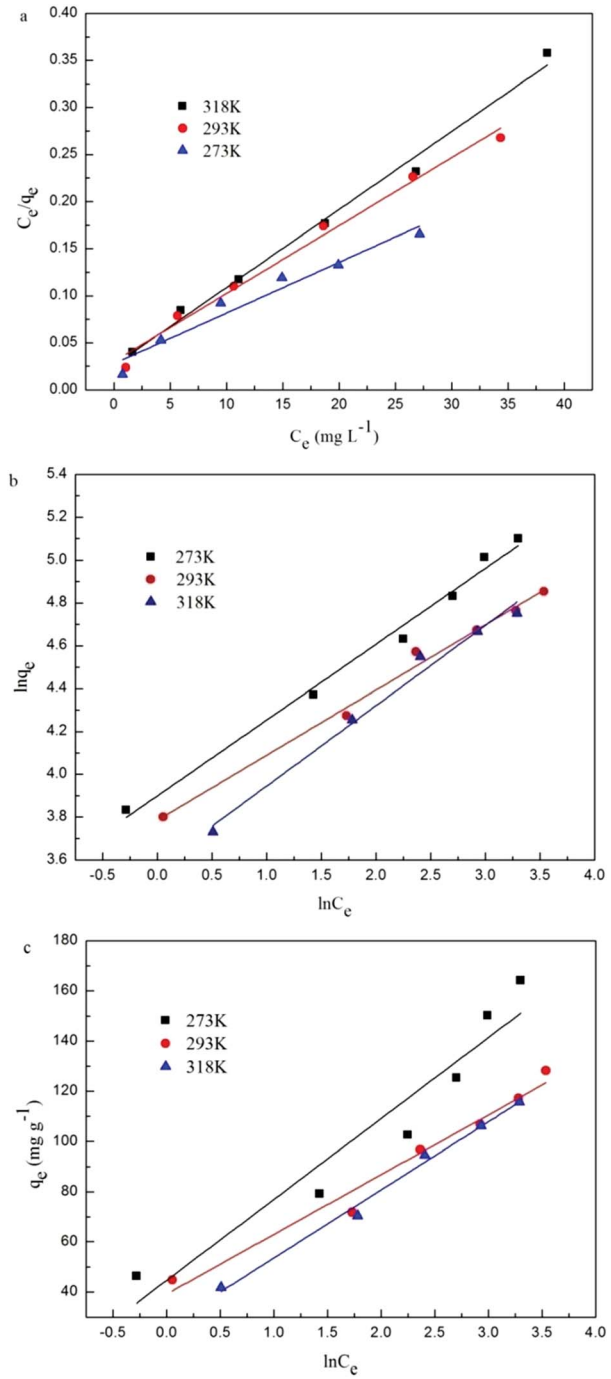

Fig. 10 (a) Langmuir, (b) Freundlich and (c) Temkin isotherms for MO adsorption onto NH_2-MWCNTs at different temperatures.

maximum MO adsorption capacity decreased from 185.53 mg g^{-1} to 120.63 mg g^{-1} with the increase in temperature from 273 K to 318 K, revealing the probability that MO adsorption by NH_2-MWCNTs is an exothermic process. This phenomenon will be further discussed in Section 3.2.8.

As also seen in Table 2, the maximum adsorption capacity was 185.53 mg g^{-1}. A comparison of q_{max} values for MO on NH_2-MWCNTs with those reported previously using various adsorbents is summarized in Table 3, which suggests that NH_2-MWCNTs hold great potential for MO removal from aqueous solutions. It is clear that NH_2-MWCNTs used in this work are an excellent adsorbent material in wastewater treatment.

Table 2 Isotherm parameters for removal of MO by NH_2-MWCNTs at different temperatures

	Langmuir			
T (K)	q_m (mg g^{-1})	B	r^2	R_L
273	185.53	0.1945	0.947	0.079–0.340
293	138.50	0.2391	0.986	0.065–0.295
318	120.63	0.3191	0.990	0.050–0.239

	Freundlich			Temkin		
T (K)	n	K_F	r^2	K_T	B	r^2
273	2.8253	49.383	0.987	3.973	32.311	0.905
293	3.2875	44.050	0.990	5.158	23.834	0.969
318	2.6661	35.532	0.981	2.635	27.183	0.989

Table 3 Maximum adsorption capacities of MO onto various adsorbents

Adsorbates	Adsorbents	q_{max} (mg g^{-1})	Ref.
MO	MWCNTS	35.4–64.7	21
	γ-Fe_2O_3/chitosan composite films	29.4	49
	Hypercrosslinked polymeric adsorbent	70	50
	Chitosan/Fe_2O_3/MWCNTs	66	51
	CNTs-A	149	20
	Silkworm exuviae	87	52
	NH_2-MWCNTs	185.5	This work

3.2.7 Adsorption kinetics. To better understand the characteristics of the adsorption process, three kinetic models including pseudo-first-order, pseudo-second-order and intraparticle diffusion model were exploited to analyze the experimental data (Fig. 11). The calculated kinetics parameters for the removal of MO with NH_2-MWCNTs are listed in Table 4.

A linear form of pseudo-first-order kinetic model might be represented by eqn (6)[51]

$$\ln(q_e - q_t) = \ln(q_e) - \frac{k_1 t}{2.302} \quad (6)$$

where q_e and q_t are the amounts of MO adsorbed at equilibrium in mg g^{-1} and at time t (min), respectively; k_1 is the rate constant of pseudo-first-order kinetic model (min^{-1}). Values of k_1 can be determined by plotting $\ln(q_e - q_t)$ against t using the eqn (6).

The pseudo-second-order kinetics can be described by the following linear equation:[53]

$$\frac{t}{q} = \frac{1}{k_2 q_e^2} + \frac{t}{q_e} \quad (7)$$

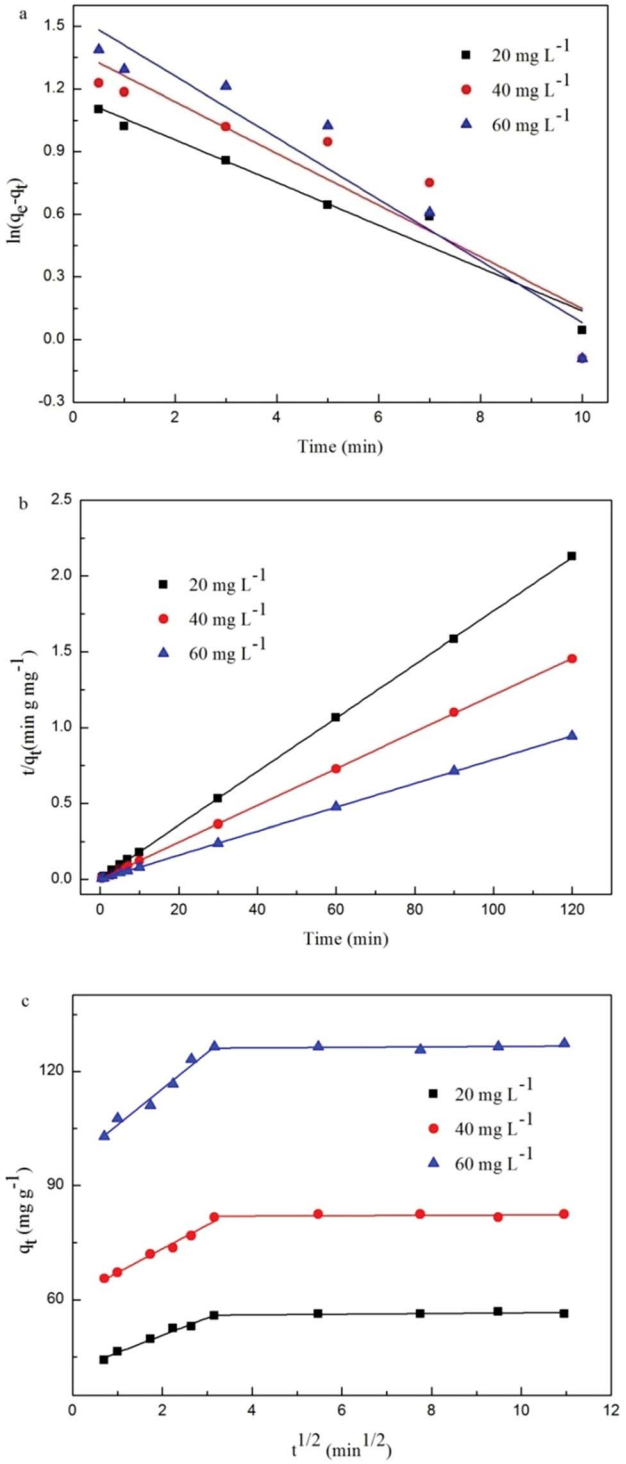

Fig. 11 Regressions of kinetic plots different initial concentrations: (a) pseudo-first-order model, (b) pseudo-second-order model and (c) intra-particle diffusion model.

where k_2 is the rate constant (g mg^{-1} min^{-1}) of pseudo-second-order kinetic model for the adsorption process. k_2 and q_e can be estimated from the slope and intercept of the linear plot of t/q_t against time as shown in Fig. 10b.

Since neither the pseudo first-order nor the second-order model can highlight on the rate-limiting step, we applied the intra-particle mass transfer diffusion model proposed by Weber–Morris. This equation can be written as follow:[54]

$$q_t = k_i t^{1/2} + C \quad (8)$$

where C (mg g^{-1}) is the intercept and k_i is the intra-particle diffusion rate constant (mg g^{-1} min$^{-1/2}$), which can be obtained by plotting q_t against $t^{1/2}$. Moreover, the values of C depict the boundary thickness.

It is noticeable that all the experimental data fitted pseudo-second-order kinetic model better in terms of higher correlation coefficient values ($R^2 > 0.999$). The q_e calculated from the pseudo-second-order kinetic model were 56.69 mg g^{-1} (20 mg L^{-1}), 83.37 mg g^{-1} (40 mg L^{-1}), and 127.06 mg g^{-1} (60 mg L^{-1}), respectively, which were rather approximate with those from the experimental results. It can be found that adsorption process could be optimum under the pseudo-second-order kinetic model.

Typically, Adsorption kinetics are controlled by various mechanisms, of which the most limiting are the diffusion mechanisms, including external diffusion and intra-particle diffusion.[55] To further predict the rate-controlling step involved in the adsorption process, the intra-particle diffusion model was utilized as shown in Fig. 11a. Piecewise linear regression of the data indicated that q_t *vs.* $t^{1/2}$ plots had two distinct regions, in which the first linear portion represented external mass transfer and the second portion related to intra-particle diffusion. There existed two steps in the overall adsorption processes: (1) the initial steep portion was a faster MO uptake due to the diffusion of adsorbate through the solution to the adsorbent external surface (external diffusion); (2) the gradual adsorption stage, which can be ascribed to diffusion of the adsorbate species from the external surface to the internal pores of the adsorbent (intra-particle diffusion).[56] As observed in Fig. 11c, the plots did not pass through the origin, implying that although intra-particle diffusion is involved in the adsorption process, it is not the unique rate-controlling step.[57] On the other hand, the stage of intra-

Table 4 Parameters of pseudo-first and second-order adsorption kinetic models and intra-particle diffusion model at various concentrations

		Pseudo-first-order model		
C_0 (mg L^{-1})	$q_{e,exp}$	k_1	q_e	r^2
20	56.35	0.236	14.53	0.94794
40	82.53	0.285	24.37	0.83325
60	127.23	0.340	36.05	0.91167

	Pseudo-second-order model			Intra-particle diffusion model		
C_0 (mg L^{-1})	k_2	q_e	r^2	k_i	C	r^2
20	0.065	56.69	0.9999	4.554	55.69	0.9815
40	0.121	82.37	0.9998	6.257	81.89	0.9786
60	0.028	127.06	0.9999	9.505	125.93	0.9704

particle diffusion is longer than external diffusion. Therefore, the whole adsorption process was controlled by not only external mass transfer but also intra-particle diffusion, in which the intra-particle diffusion prevailed over the external mass transfer.

3.2.8 Thermodynamic studies. To assess the influence of temperature on the adsorption process of MO onto NH_2-MWCNTs, thermodynamic parameters such as the standard free energy change (ΔG^0), standard enthalpy change (ΔH^0), and standard entropy change (ΔS^0) were determined from the variation of the thermodynamic equilibrium constant K_0 with the change in temperature.[58]

For the sorption reactions, the constant K_0 can be defined as follows:[59]

$$K = \frac{a_s}{a_e} = \frac{\gamma_s}{\gamma_e}\frac{q_e}{C_e} \quad (9)$$

where a_s is the activity of sorbed MO; a_e is the activity of MO in solution at equilibrium; γ_s is the activity coefficient of the adsorbed MO; γ_e is the activity coefficient of MO in solution at equilibrium. As the concentration of MO in the solution decreases and approaches zero, the activity coefficient approaches unity, therefore, values of K_0 can be obtained by plotting the $\ln\left(\frac{q_e}{C_e}\right)$ *versus* q_e and extrapolating q_e to zero as shown in Fig. S2.†

The adsorption standard Gibbs free energy changes (ΔG^0) for any interaction can be calculated using the following relationships:

$$\Delta G^0 = -RT \ln K_0 \quad (10)$$

$$\Delta G^0 = \Delta H^0 - T\Delta S^0 \quad (11)$$

By rearranging the eqn (6) and (7), K_0 may be obtained using the relationship as follows:

$$\ln K_0 = -\frac{\Delta H^0}{RT} + \frac{\Delta S^0}{R} \quad (12)$$

where R is the gas constant (8.314 J mol^{-1} K^{-1}), and T is the adsorption temperature in Kelvin. ΔH^0 and ΔS^0 can be calculated from the slope $\left(-\frac{\Delta H^0}{RT}\right)$ and the intercept $\left(\frac{\Delta S^0}{R}\right)$ of the Van't Hoff plot of $\ln K_0$ *versus* $(1/T)$ as shown in Fig. S3† and are listed in Table 5.

The negative ΔG^0 values at all temperature confirm the feasibility of the process and the spontaneous nature of the adsorption. The change in free energy for physisorption is generally in the range of 0 to −20 kJ mol^{-1} and chemisorptions occur within the range −80 to −400 kJ mol^{-1}.[60] The calculated ΔG^0 values indicate that the interaction between MO and NH_2-MWCNTs can be considered to be physical in nature. In this study, the observed negative ΔH^0 showed an exothermic adsorption, which was supported by the phenomenon that the sorption of MO decreased with the increase of sorption temperature (Fig. 9). It is generally accepted that ΔH^0 ranges of physical and chemical adsorptions are 2–21 and 80–200 kJ mol^{-1}, respectively.[61] From this point of view, the magnitude of ΔH^0 is −15 kJ mol^{-1}, suggesting the adsorption of MO onto NH_2-MWCNTs is mainly physical in nature, which is in accordance with the results discussed above. The negative value of ΔS^0 corresponded to a decrease of randomness in solid–liquid interface during the adsorption process. It thus contributed to the decrease of MO sorption capacities at higher temperature.

Table 5 Values of thermodynamic parameters for the adsorption of MO dye on NH_2-MWCNTs

T (K)	$\ln K_0$	ΔG^0 (kJ mol^{-1})	ΔH^0 (kJ mol^{-1})	ΔS^0 (J mol^{-1} K^{-1})
273	5.129	−11.624		
293	4.845	−11.803	−15.434	−13.469
318	4.168	−11.03		

4. Conclusions

Amino-functionalization of MWCNTs for the removal of MO from aqueous solution was successfully prepared using 1,6-hexanediamine *via* a simple one-pot synthesis. The FTIR, XPS and elemental analysis results of the samples confirmed that amine have successfully grafted onto the surface of MWCNTs.

To the best of our knowledge, this study is the first to synthesize NH_2-MWCNTs by solvothermal method and use it as adsorbent for MO removal. The adsorption process was systematically researched under different conditions. The initial pH values of solutions have a remarkable influence on the adsorption capacity, which increased with the decrease of pH. NH_2-MWCNTs are quite effective removal materials for the fast removal of MO and the equilibrium could be reached within 10 min at 298 K when the initial concentration of MO was 60 mg L^{-1}. Three kinds of isotherms equation were utilized to fit the experimental data and the maximum adsorption capacity calculated from the Langmuir model was 185.53 mg g^{-1}.

At the same time, the adsorption kinetic was more accurately fitted with pseudo-second-order model. The results of intra-particle diffusion model indicated that the overall process appeared to be jointly controlled by intra-particle diffusion and external mass transfer. Additionally, thermodynamic analyses revealed that the adsorption of MO onto NH_2-MWCNTs was exothermic and spontaneous at the temperature studied.

The results obtained in this work suggested that the amino-functionalized multi-walled carbon nanotubes could be regarded as a potential candidate for high efficient adsorbent for MO in practical application. Furthermore, the amino groups grafted on surfaces of MWCNTs using a simple one-pot method may provide a good idea for developing other promising materials for the removal of MO from wastewater.

Acknowledgements

We thank Mr Jie Wei for giving many suggestions on this work.

Notes and references

1 V. K. Gupta, I. Ali, T. A. Saleh, A. Nayak and S. Agarwal, *RSC Adv.*, 2012, **2**, 6380–6388.
2 S. Zhang, J. Li, T. Wen, J. Xu and X. Wang, *RSC Adv.*, 2013, **3**, 2754–2764.
3 S. Zhang, W. Xu, M. Zeng, J. Li, J. Li, J. Xu and X. Wang, *J. Mater. Chem. A*, 2013, **1**, 11691–11697.
4 S. Karthikeyan, V. K. Gupta, R. Boopathy, A. Titus and G. Sekaran, *J. Mol. Liq.*, 2012, **173**, 153–163.
5 H. L. Parker, A. J. Hunt, V. L. Budarin, P. S. Shuttleworth, K. L. Miller and J. H. Clark, *RSC Adv.*, 2012, **2**, 8992–8997.
6 A. Mittal, D. Kaur, A. Malviya, J. Mittal and V. K. Gupta, *J. Colloid Interface Sci.*, 2009, **337**, 345–354.
7 A. Mittal, J. Mittal, A. Malviya and V. K. Gupta, *J. Colloid Interface Sci.*, 2009, **340**, 16–26.
8 A. Mittal, J. Mittal, A. Malviya, D. Kaur and V. K. Gupta, *J. Colloid Interface Sci.*, 2010, **342**, 518–527.
9 M. Biswal, K. Bhardwaj, P. K. Singh, P. Singh, P. Yadav, A. Prabhune, C. Rode and S. Ogale, *RSC Adv.*, 2013, **3**, 2288–2295.
10 V. K. Gupta, R. Jain, A. Mittal, T. A. Saleh, A. Nayak, S. Agarwal and S. Sikarwar, *Mater. Sci. Eng., C*, 2012, **32**, 12–17.
11 T. A. Saleh and V. K. Gupta, *J. Colloid Interface Sci.*, 2012, **371**, 101–106.
12 V. K. Gupta, R. Jain, A. Nayak, S. Agarwal and M. Shrivastava, *Mater. Sci. Eng., C*, 2011, **31**, 1062–1067.
13 V. K. Gupta, B. Gupta, A. Rastogi, S. Agarwal and A. Nayak, *J. Hazard. Mater.*, 2011, **186**, 891–901.
14 Y.-Y. Xu, M. Zhou, H.-J. Geng, J.-J. Hao, Q.-Q. Ou, S.-D. Qi, H.-L. Chen and X.-G. Chen, *Appl. Surf. Sci.*, 2012, **258**, 3897–3902.
15 V. K. Gupta and A. Nayak, *Chem. Eng. J.*, 2012, **180**, 81–90.
16 A. Mittal, J. Mittal, A. Malviya and V. K. Gupta, *J. Colloid Interface Sci.*, 2010, **344**, 497–507.
17 R.-S. Juang, G. Annadurai and D.-J. Lee, *J. Hazard. Mater.*, 2002, **92**, 263–274.
18 S. Chen, J. Zhang, C. Zhang, Q. Yue, Y. Li and C. Li, *Desalination*, 2010, **252**, 149–156.
19 Y. Haldorai and J.-J. Shim, *Appl. Surf. Sci.*, 2014, **292**, 447–453.
20 J. Ma, F. Yu, L. Zhou, L. Jin, M. Yang, J. Luan, Y. Tang, H. Fan, Z. Yuan and J. Chen, *ACS Appl. Mater. Interfaces*, 2012, **4**, 5749–5760.
21 Y. Yao, H. Bing, X. Feifei and C. Xiaofeng, *Chem. Eng. J.*, 2011, **170**, 82–89.
22 S. Iijima, *Nature*, 1991, **354**, 56–58.
23 C. Luo, Z. Tian, B. Yang, L. Zhang and S. Yan, *Chem. Eng. J.*, 2013, **234**, 256–265.
24 C. Luo, R. Wei, D. Guo, S. Zhang and S. Yan, *Chem. Eng. J.*, 2013, **225**, 406–415.
25 G. Zhao, T. Wen, C. Chen and X. Wang, *RSC Adv.*, 2012, **2**, 9286–9303.
26 T. A. Saleh and V. K. Gupta, *Environ. Sci. Pollut. Res.*, 2012, **19**, 1224–1228.
27 V. K. Gupta, S. K. Srivastava, D. Mohan and S. Sharma, *Waste Manage.*, 1997, **17**, 517–522.
28 H. Khani, M. K. Rofouei, P. Arab, V. K. Gupta and Z. Vafaei, *J. Hazard. Mater.*, 2010, **183**, 402–409.
29 V. K. Gupta, S. Agarwal and T. A. Saleh, *J. Hazard. Mater.*, 2011, **185**, 17–23.
30 G. D. Vuković, A. D. Marinković, M. Čolić, M. Đ. Ristić, R. Aleksić, A. A. Perić-Grujić and P. S. Uskoković, *Chem. Eng. J.*, 2010, **157**, 238–248.
31 G. Vuković, A. Marinković, M. Obradović, V. Radmilović, M. Čolić, R. Aleksić and P. S. Uskoković, *Appl. Surf. Sci.*, 2009, **255**, 8067–8075.
32 Z. Zang, Z. Hu, Z. Li, Q. He and X. Chang, *J. Hazard. Mater.*, 2009, **172**, 958–963.
33 J. Yu, M. Tong, X. Sun and B. Li, *React. Funct. Polym.*, 2007, **67**, 564–572.
34 F. Su, C. Lu and S. Hu, *Colloids Surf., A*, 2010, **353**, 83–91.
35 L. Lai, L. Chen, D. Zhan, L. Sun, J. Liu, S. H. Lim, C. K. Poh, Z. Shen and J. Lin, *Carbon*, 2011, **49**, 3250–3257.
36 S. Stankovich, D. A. Dikin, R. D. Piner, K. A. Kohlhaas, A. Kleinhammes, Y. Jia, Y. Wu, S. T. Nguyen and R. S. Ruoff, *Carbon*, 2007, **45**, 1558–1565.
37 A. Mas, H. Jaaba and F. Schue, *Macromol. Chem. Phys.*, 1997, **198**, 3737–3752.
38 M. Okubo, Y. Yamamoto and S. Kamei, *Colloid Polym. Sci.*, 1989, **267**, 861–865.
39 L. Lai, G. Huang, X. Wang and J. Weng, *Carbon*, 2010, **48**, 3145–3156.
40 T.-L. Wang and C.-G. Tseng, *J. Appl. Polym. Sci.*, 2007, **105**, 1642–1650.
41 K. Bhattacharyya and A. Sharma, *Dyes Pigm.*, 2005, **65**, 51–59.
42 M.-S. Chiou, P.-Y. Ho and H.-Y. Li, *Dyes Pigm.*, 2004, **60**, 69–84.
43 F. Yu, J. Chen, L. Chen, J. Huai, W. Gong, Z. Yuan, J. Wang and J. Ma, *J. Colloid Interface Sci.*, 2012, **378**, 175–183.
44 O. Hamdaoui and E. Naffrechoux, *J. Hazard. Mater.*, 2007, **147**, 401–411.
45 I. Langmuir, *J. Am. Chem. Soc.*, 1918, **40**, 1361–1403.
46 K. R. Hall, L. C. Eagleton, A. Acrivos and T. Vermeulen, *Ind. Eng. Chem. Fundam.*, 1966, **5**, 212–223.
47 M. Ahmaruzzaman and S. Laxmi Gayatri, *Chem. Eng. J.*, 2010, **158**, 173–180.
48 S. J. Allen, G. McKay and J. F. Porter, *J. Colloid Interface Sci.*, 2004, **280**, 322–333.
49 R. Jiang, Y.-Q. Fu, H.-Y. Zhu, J. Yao and L. Xiao, *J. Appl. Polym. Sci.*, 2012, **125**, E540–E549.
50 J.-H. Huang, K.-L. Huang, S.-Q. Liu, A. T. Wang and C. Yan, *Colloids Surf., A*, 2008, **330**, 55–61.
51 H. Y. Zhu, R. Jiang, L. Xiao and G. M. Zeng, *Bioresour. Technol.*, 2010, **101**, 5063–5069.
52 H. Chen, J. Zhao, J. Wu and G. Dai, *J. Hazard. Mater.*, 2011, **192**, 246–254.
53 Y. S. Ho and G. McKay, *Chem. Eng. J.*, 1998, **70**, 115–124.
54 D. Kavitha and C. Namasivayam, *Bioresour. Technol.*, 2007, **98**, 14–21.
55 A. Ozcan, E. M. Oncu and A. S. Ozcan, *J. Hazard. Mater.*, 2006, **129**, 244–252.

56 B. Chen, Z. Zhu, J. Ma, Y. Qiu and J. Chen, *J. Mater. Chem. A*, 2013, **1**, 11355–11367.
57 M. Dogan, H. Abak and M. Alkan, *J. Hazard. Mater.*, 2009, **164**, 172–181.
58 R. Niwas, U. Gupta, A. A. Khan and K. G. Varshney, *Colloids Surf., A*, 2000, **164**, 115–119.
59 I. I. Fasfous, E. S. Radwan and J. N. Dawoud, *Appl. Surf. Sci.*, 2010, **256**, 7246–7252.
60 Y. Yu, Y.-Y. Zhuang, Z.-H. Wang and M.-Q. Qiu, *Chemosphere*, 2004, **54**, 425–430.
61 Y. Liu and Y.-J. Liu, *Sep. Purif. Technol.*, 2008, **61**, 229–242.